Internal Physical Features of a Land Surface Model Employing a Tangent Linear Model

Runhua Yang*, Stephen E. Cohn, Arlindo da Silva, Joanna Joiner, Paul R. Houser

Data Assimilation Office
NASA/GSFC
Greenbelt, MD 20771

* Additional affiliation: General Sciences Corporation, a subsidiary of Science Applications International Corporation, Laurel, MD

Abstract:

The Earth's land surface, including its biomass, is an integral part of the Earth's weather and climate system. Land surface heterogeneity, such as the type and amount of vegetative covering, has a profound effect on local weather variability and therefore on regional variations of the global climate.

Surface conditions affect local weather and climate through a number of mechanisms. First, they determine the re-distribution of the net radiative energy received at the surface, through the atmosphere, from the sun. A certain fraction of this energy increases the surface ground temperature, another warms the near-surface atmosphere, and the rest evaporates surface water, which in turn creates clouds and causes precipitation. Second, they determine how much rainfall and snowmelt can be stored in the soil and how much instead runs off into waterways. Finally, surface conditions influence the near-surface concentration and distribution of greenhouse gases such as carbon dioxide.

The processes through which these mechanisms interact with the atmosphere can be modeled mathematically, to within some degree of uncertainty, on the basis of underlying physical principles. Such a land surface model provides predictive capability for surface variables including ground temperature, surface humidity, and soil moisture and temperature. This information is important for agriculture and industry, as well as for addressing fundamental scientific questions concerning global and local climate change.

In this study we apply a methodology known as tangent linear modeling to help us understand more deeply the behavior of the Mosaic land surface model, a model that has been developed over the past several years at NASA/GSFC. This methodology allows us to examine, directly and quantitatively, the dependence of prediction errors in land surface variables upon different vegetation conditions. The work also highlights the importance of accurate soil moisture information. Although surface variables are predicted imperfectly due to inherent uncertainties in the modeling process, our study suggests how satellite observations can be combined with the model, through land surface data assimilation, to improve their prediction.

Internal Physical Features of the Mosaic Land Surface Model Employing Tangent Linear Model Analysis

Runhua Yang*, Stephen E. Cohn, Arlindo da Silva, Joanna Joiner, Paul R. Houser

Data Assimilation Office

NASA/GSFC

Greenbelt, MD 20771

*Additional affiliation: General Sciences Corporation, a subsidiary of Science Applications International Corporation, Laurel, MD

Will be submitted to Monthly Weather Review

Abstract:

We explore the internal dynamical and physical features of the Mosaic land surface model (LSM, Koster and Suarez 1992) using a tangent linear model (TLM) eigenanalysis. The integration with the Mosaic LSM is performed for both grass and bare soil land covers with the atmospheric boundary forcing conditions observed at the Hapex-Mobilhy Caumont site in France. The TLM is derived numerically by finite differencing with realistic values of the basic state. The eigenvalues of this TLM represent characteristic time scales of land surface state perturbations, and the scaled eigenvectors (modes) illustrate the coupling among the land surface state perturbations. The results suggest that: (1) the Mosaic land surface model is stable for the considered basic state, i.e., any initial perturbation, or initial error, will decay with time. The constraints based on physical principles in the Mosaic LSM prevent instabilities of the land surface state perturbations. (2) The time scales of land surface state perturbations range from a few minutes to several months. Modes mainly representing the behavior of surface temperature and surface moisture perturbations exhibit short time scales, whereas the modes mainly representing soil moisture transfer between the root and deep model layers exhibit long time scales. (3) The time scales of the modes depend significantly upon vegetation parameters, soil hydraulic parameters, and soil layer structure.

TLM eigenanalysis provides quantitative estimates of the time scales and structure of the land surface state perturbations. It is an efficient and effective tool for developing the understanding of the Mosaic LSM internal features. Moreover, it provides useful insight for error covariance modeling needed in land surface data assimilation.

1. Introduction

A land surface model or soil-vegetation-atmosphere-transfer (SVAT) scheme exhibits a wide range of variability on time scales from hours to months, and even years through atmospheric interactions (Delworth and Manabe 1988, 1993; Entekhabi 1995). These time scales are strongly controlled by external forcing terms, especially precipitation and downward short-wave and long-wave radiation at the surface. They are also modulated by the internal dynamics and physics of land surface systems, in particular soil moisture dynamics. There are numerous studies on the variability of land surface models. Common approaches to date include: 1) performing numerical simulations, 2) building relatively simple land surface systems that can be solved analytically, and 3) performing numerical sensitivity tests.

In the first approach, either a General Circulation Model (GCM) including a land surface model or a stand-alone land surface model is integrated over long periods (e.g., Dickinson et al. 1984; Sato et al. 1989). These studies have demonstrated the main variability of the land surface system and the pronounced effect of the land surface on atmospheric variability. The second approach, solving equations of a simple land surface model analytically, estimates characteristic time scales of land surface variables in extreme or simplified cases (e.g., Delworth and Manabe 1988; Brubaker and Entekhabi 1995; Yang et al. 1995). This approach greatly simplifies complex land surface processes. For example, one can represent the evaporation and runoff process as a bucket model or treat the soil moisture system as a first-order Markov process. However, such approximations may represent an oversimplification of land surface processes. In the third approach, using either a coupled GCM or stand-alone land surface model, sensitivity experiments are usually performed with a change in one particular parameter or parameterization scheme (e.g., Henderson-Sellers et al. 1995; Xue et al. 1996a, 1996b). The results are then compared with a control integration, to reveal the impact of the change. This type of sensitivity experiment identifies important parameters or parameterizations in land surface models.

These three approaches do not disclose much information about variability due solely to the *internal* dynamics and physics in land surface models. They mainly reveal the impact of external forcing variability, due to the dominant control of the forcing terms (Entekhabi 1995; Delworth and Manabe 1988, 1993). Even in sensitivity tests, the signature of internal dynamics and physics is embedded within that of external forcing variability.

Understanding of the internal dynamics and physics of a land surface model is important for the development of land surface data assimilation methods. First, under the tangent linear approximation, the internal dynamics and physics alone control land surface state perturbations, which are defined as the departures from a nonlinear model trajectory. Second, with an understanding of the internal features, we can readily identify key parameters and parameterizations that affect land surface state variations with minimum influence of the external forcing.

In this study, we explore the application of tangent linear model (TLM) analysis to the internal physics and dynamics of the Mosaic Land Surface Model (LSM, Koster and Suarez 1992). In a recent review paper, Errico (1997) describes the development and applications of tangent linear models in meteorology. A tangent linear model, together with its adjoint model, is an exceptionally powerful tool for solving many meteorological problems. Its main applications include sensitivity analysis of atmospheric system, optimal analysis in the data assimilation, and dynamic stability analysis. Though the use of tangent linear models and adjoint models has been increasing rapidly during the last decade, the application to land surface models is not yet common. In this paper we present the TLM development and eigenanalysis for the Mosaic LSM. The results show that TLM eigenanalysis provides a effective method for understanding the internal features of the Mosaic LSM.

In Section 2 we briefly describe the Mosaic land surface model. In Section 3, we derive the tangent linear model based on the prognostic equations of the Mosaic LSM, and we describe the experimental

design and precautions taken in deriving the TLM numerically. In Section 4 we present the results of the TLM eigenanalysis, including characteristic time scales and modes of the land surface state perturbations. In Section 5, we obtain a linearized soil moisture subsystem and examine the role of soil moisture dynamics. We further simplify this subsystem to find explicit relationships between the eigenvalues and the Mosaic LSM parameters. Finally, in Section 6 we summarize the main results and discuss their application to land surface data assimilation.

2. Description of Mosaic Land Surface Model

The Mosaic LSM (Koster and Suarez 1992) is named for its use of the "mosaic" strategy to account for subgrid heterogeneity in surface characteristics. In the Mosaic LSM, every surface grid cell in a GCM is subdivided into relatively homogeneous subregions, or "mosaic tiles". Each tile contains a single vegetation or bare soil type. Energy and water balance calculations are performed over each tile. The tiles in a grid cell respond to the mean conditions in the overlaying GCM grid cell. This GCM grid cell, in turn, responds to the area-weighted fluxes of heat and moisture from the tiles (Koster and Suarez 1996).

The Mosaic LSM is based on the Simple Biosphere (SiB) model of Sellers et al. (1986), and includes sophisticated biophysical processes. Similar to SiB, it calculates the energy and water transfers using an electrical resistance network analog (Fig. 1). For example, to calculate the latent heat flux (current) along a given pathway, the difference between surface and atmospheric vapor pressures (potentials) is divided by an effective resistance, which is a function of the atmospheric conditions, and plant and soil properties. Similarly, the sensible heat flux is determined by the difference between the temperatures (potentials) of the surface and the boundary atmosphere. Recently the Mosaic LSM has been successfully implemented into the Goddard Earth Observing System General Circulation Model (GEOS GCM) at the Data Assimilation Office of the NASA Goddard Space Flight Center (DAO 1996).

The eight prognostic variables in each tile of the Mosaic LSM are:

T_c: temperature of the surface/canopy system

T_d: temperature in deep soil

C: moisture in the canopy interception reservoir

W_i (i=1,2,3): moisture in the top, middle, and the bottom soil layers, respectively

S: water equivalent in the snowpack, if any

e_a: vapor pressure in near surface layer (within the canopy for the vegetation tiles).

The prognostic equations are as follows:

$$C_{II}\frac{\delta T_c}{\Delta t} = R_{sw-net} + R_{lw}^{\downarrow} - R_{lw}^{\uparrow} - H - \lambda E - G_d, \tag{1}$$

$$C_{II-deep}\frac{\delta T_d}{\Delta t} = G_d, \tag{2}$$

$$\frac{\delta C}{\Delta t} = P + S_{melt} - E_{int} - P_T, \tag{3}$$

$$\frac{\delta W_1}{\Delta t} = P_T - R_s - E_{bs} - E_{transp,1} - Q_{1,2}, \tag{4}$$

$$\frac{\delta W_2}{\Delta t} = Q_{1,2} - E_{transp,2} - Q_{2,3}, \tag{5}$$

$$\frac{\delta W_3}{\Delta t} = Q_{2,3} - Q_{3,\infty}, \tag{6}$$

$$\frac{\delta S}{\Delta t} = P_s - S_{melt} - E_{snow}. \tag{7}$$

The prognostic equation for surface layer or canopy air vapor pressure (e_a) is obtained by differentiating the following diagnostic equation for surface evaporation E with respect to T_c and e_a:

$$E = \frac{\rho\epsilon}{p_s}\left[\frac{e_s(T_c) - e_a}{r_{eff}(T_c, e_a)}\right]. \tag{8}$$

The details of the derivation are given in Koster and Suarez (1992, 1994, 1996).

The terms in the equations are:

Δt: model time step

C_{II}: heat capacity of surface/canopy system

R_{sw-net}: net short-wave radiation at surface

$R_{lw}^{\downarrow}$: downward long-wave radiation at surface

$R_{lw}^{\uparrow}$: upward long-wave radiation at surface

H: sensible heat flux

λE: latent heat flux

G_d: heat flux to deep soil

$C_{II-deep}$: heat capacity of deep soil system

P: precipitation rate

S_{melt}: snow-melt rate

E_{int}: evaporation of intercepted water

P_T: throughfall rate of precipitation

R_s: surface runoff rate

E_{bs}: evaporation rate from surface

$E_{transp,i}$ (i=1,2): water removal rate via transpiration from the ith soil layer

$Q_{i,j}$: moisture flux from ith soil layer to jth soil layer

P_s: snow fall rate

E_{snow}: snow sublimation rate

e_s: saturated vapor pressure, a function of T_c

r_{eff}: effective surface resistance to vapor transport, a function of T_c and e_a

ρ: air density

ϵ: ratio of the molecular weight of water vapor to that of dry air

p_s: surface pressure

3. TLM derivation and experimental design

a. Tangent linear model derivation

Let X denote the vector of prognostic (state) variables. Written as a system of eight ordinary differential equations, the general form of equations (1)-(8) is

$$\frac{dX}{dt} = F(X) + \text{external forcing}, \tag{9}$$

where the vector $F(X)$ can be represented by $F(X) = (F_1, F_2, ..., F_8)^T$, and the superscript T denotes the transpose. External forcing terms are the near-surface atmospheric conditions, such as precipitation and downward solar and longwave radiation fluxes at the surface. These terms do not depend explicitly on the land surface state X.

A perturbation method is used to linearize the nonlinear system (9). A solution X of equation (9) is decomposed into a "*basic state*" $\bar{X} = \bar{X}(t)$ satisfying (9), plus a perturbation X':

$$X = \bar{X} + X'. \tag{10}$$

The Taylor expansion of F around the basic state $\bar{X}$ is

$$F_i(X) = F_i(\bar{X}) + \sum_j \left(\left. \frac{\partial F_i}{\partial X_j} \right|_{X_j = \bar{X}_j} \right) X'_j + O(X'^2). \tag{11}$$

Substituting equations (10) and (11) into the system (9) and neglecting the higher-order terms, we obtain the tangent linear model:

$$\frac{dX'}{dt} = AX', \tag{12}$$

where $A_{ij} \equiv \left(\left. \frac{\partial F_i}{\partial X_j} \right|_{X_j = \bar{X}_j} \right)$, and $A = A(\bar{X}(t))$ is the tangent linear matrix or Jacobian. In a data assimilation context, the basic state $\bar{X}$ denotes a nonlinear model trajectory, and the linear system (12) approximates the evolution of an initial error $X'(0) = X'(t = 0)$ in that trajectory. Since the linear system

(12) eliminates the external forcing term, the behavior of $X'(t)$ is determined by the internal physics and dynamics of the Mosaic LSM in the vicinity of the basic state. Dependence of $X'(t)$ on the external forcing is implicit, through the dependence of $A(\bar{X}(t))$ on the basic state.

We study the behavior of (12) for A evaluated either at a specific time or for a specific time-mean state. This simplifies the problem considerably, for in each case A is then independent of time. The solution of (12) is just

$$X'(t) = e^{At}X'(0). \tag{13}$$

The eigendecomposition of A is given by

$$A = U\Lambda U^{-1}, \tag{14}$$

where Λ is the diagonal matrix of eigenvalues of A, and the columns of U are the corresponding eigenvectors. An eigenvector (mode) corresponding to a given eigenvalue expresses a specific coupling among the variables $X'(t)$.

Since we consider A to be independent of time, the stability of the linear system (12) depends on the eigenvalues Λ. If all eigenvalues have negative real parts, the system is stable for the basic state we consider, and any initial error will decay with time; if any one of the eigenvalues has a positive real part, the system is unstable. If all eigenvalues are real, the solutions are non-oscillatory. A negative eigenvalue λ represents a decay rate with e-folding time $\tau = \frac{-1}{\lambda}$.

b. Experimental design

We perform four experiments with two considerably different sets of vegetation parameters and basic states. The purpose is to examine the characteristic time scales and the coupling of land surface state perturbations or errors, under different land surface conditions and basic states. In experiments one and two (EXP 1, EXP 2), the vegetation type is grass, with two different basic states. In experiments three and four (EXP 3, EXP 4), the vegetation type is bare soil, and the same basic states of EXP 1 and EXP

2 are used.

We first generated a 3-year long control integration with 90% grass and 10% bare soil using one year of observed surface forcing repeatedly. The purpose of the control run is two-fold. First, it shows the length of time required for the Mosaic LSM to arrive at equilibrium. Second, it provides appropriate basic state values for the four experiments. We selected values for the basic state from the control run after equilibrium was reached.

The near-surface atmospheric forcing for the control run was observed at the Hapex-Mobilhy Caumont site, in France ($43^0 41'' N$, $0^0 6''$ W) (Goutorbe 1991; Goutorbe and Tarrieu 1991). The data are available at 30-minute time intervals for 1986. When the data were unavailable, neighboring meteorological stations were selected to provide the required information. This data set has been used in the Project of Intercomparison of Land surface Processes Phase 2 (PILPS-2) experiments (Henderson-Sellers et al., 1993). The forcing terms include downward shortwave and longwave radiation, precipitation, air temperature, 2-meter specific humidity, 2-meter wind speed, and surface pressure.

We found that the Mosaic LSM reaches an equilibrium state in about six months. Therefore, we use the results from the second year of the control run. Figure 2 shows the monthly-mean diurnal cycle of the land surface variables for June. It represents a typical example for middle latitude regions. The canopy air vapor pressure (e_a) is consistently higher than the 2-meter vapor pressure (e_{2m}) with strong diurnal variability. The surface canopy temperature (T_c) is higher than that at 2-meter (T_{2m}) during the day with a peak difference around noon. At night, the surface temperature becomes lower than that at 2-meter as a result of longwave emission from the surface. The deep soil temperature (T_d) does not change much. The soil wetness of the first two layers, which is defined as the degree of saturation in each respective soil layer, is dryer than in the deep layer, since evaporation and evapotranspiration take place from the first two layers. Only the surface layer exhibits a significant soil wetness diurnal cycle.

Based on this long-term control run, we selected two basic states: the state at 13Z June 1, 1986, and the June monthly mean state at 13Z. The other input parameters to the TLM correspond to these two situations. We select noontime and a summer month, June, since the land surface processes are most active then. Due to the lack of snow cover and interception storage during these times, the original eight prognostic equations are reduced to six equations. The counterparts of equations (3) and (7) are therefore eliminated from the TLM (equation 12).

Table 1 summarizes the four experiments, together with the two basic states, leaf area index, and soil physical parameters. There are clear differences between the two basic states: the temperature and surface vapor pressure values at 13Z mean for June are higher than at 13Z June 1, and all three soil wetness values at 13Z mean for June are consistently lower than those at 13Z June 1. The vegetation and soil parameters are also significantly different between grass and bare soil. The "scaling values" in Table 1 are described in the next subsection.

c. Tangent linear matrix calculation

The tangent linear matrices $A(\bar{X})$ for the four experiments were calculated using a centered difference schemes, rather than an analytical derivative, as follows. For each experiment, six pairs of perturbed states $(\bar{X}+\delta x_j)$ and $(\bar{X}-\delta x_j)$, $j = 1, 2, ..., 6$ are formed first. Here $\bar{X}$ is the basic state and δx_j is a perturbation, described below, around the j^{th} component of the basic state. Six pairs of one-step integrations with the Mosaic LSM are then performed, to compute $\frac{F_i(\bar{X}+\delta x_j)-F_i(\bar{X}-\delta x_j)}{2\delta x_j}$ as an approximation to $A_{ij}(\bar{X})$ for $i, j = 1, 2, ..., 6$. Then the perturbation magnitude is reduced by a factor of two and the process is repeated. At the n^{th} step, $\delta x_j = \frac{\delta x_j{}^1}{2^{(n-1)}}$ for $j = 1, 2, ..., 6$, where $\delta x_j{}^1$ is the perturbation at the initial step. The process is halted when the successive matrices show sufficient convergence of their eigenvalues, as described in the following section. Thus we arrive at $A(\bar{X})$ for each of the four experiments.

The magnitudes of the initial perturbations should be meaningful, for example, not larger than the

Table 1: Experiment description. SW_i is soil wetness (the degree of saturation, $W_i/W_{i,sat}$) , and $W_{i,sat}$ is the saturation moisture content in i_{th} soil layer. $\delta Z_{i,j}$ is the distance between the centers of i_{th} and j_{th} soil layer. LAI is the leaf area index.

ITEM	EXP 1	EXP 2	EXP 3	EXP 4
Description of basic state and forcing terms	basic state and forcing terms from: 13Z June 1, 1986	basic state and forcing terms from: 13Z mean for June	basic state and forcing terms from: 13Z June 1, 1986	basic state and forcing terms from: 13Z mean for June
Vegetation type	grass	grass	bare soil	bare soil
Basic states:				
T_c (K)	18.27	26.08	18.27	26.08
T_d (K)	16.53	17.72	16.53	17.72
e_a (hpa)	18.95	22.64	18.95	22.64
SW_1	0.5439	0.4143	0.5439	0.4143
SW_2	0.5782	0.4948	0.5782	0.4948
SW_3	0.6910	0.6244	0.6910	0.6244
Parameters:				
LAI	3.671	3.671	0.001	0.001
$W_{1,sat}(mm)$	8.4	8.4	4.0	4.0
$W_{2,sat}(mm)$	197.4	197.4	4.0	4.0
$W_{3,sat}(mm)$	420.0	420.0	130.56	130.56
$\delta Z_{1,2}(m)$	0.245	0.245	0.0092	0.0092
$\delta Z_{2,3}(m)$	0.735	0.735	0.1546	0.1546
Scaling Value:				
for T_c (K)	5.6	5.6	9.0	9.0
for T_d (K)	1.53	1.53	2.13	2.13
for e_a (hpa)	5.0	5.0	3.7	3.7
for W_1 (mm)	0.59	0.59	0.52	0.52
for W_2 (mm)	11.10	11.10	0.375	0.375
for W_3 (mm)	17.34	17.34	5.23	5.23

size of uncertainties in the land surface state. Also the perturbed states should stay within the local linear regime of the basic state. As shown in the control run, the basic state at noon time satisfies the relationships $SW_3 > SW_2 > SW_1$, $T_c > T_{2m}$, and $e_a > e_{2m}$. The perturbed states should retain these relationships to stay within the linear regime. There are also numerous "conditionals" in the formulation of the Mosaic LSM. For example, soil moisture diffusion between two adjacent layers depends on the moisture gradient. If the perturbed state reverses this gradient, the soil moisture flux will abruptly change sign and magnitude. We carefully chose the perturbation magnitudes so that the perturbed states lie within the same continuous regime as the basic state. The initial perturbation magnitude was one degree Celsius for T_c and T_d, one hpa for e_a, 3% for the first and second layer soil wetness, and 5% for deep soil wetness.

An eigenanalysis will be applied to each of the four matrices $A(\bar{X})$ as described in Section 4. The eigenvectors are scaled to nondimensionalize and to enable to comparison of their elements, and are also normalized to unity upon dividing by the largest magnitude of the respective eigenvector elements. For EXP 1 and EXP 2, we select the scaling magnitudes as the standard deviations of each state variable at 13Z over the month of June from the control run. For EXP 3 and EXP 4, we performed a second control run with bare soil to obtain scaling magnitudes, since the standard deviations differ from the control run with grass (see scaling values in Table 1). The standard deviations at 13Z of June from this second control run are selected as the scaling magnitudes for EXP 3 and EXP 4.

4. Eigenanalysis of the tangent linear matrix

a. Eigenanalysis for the two experiments with vegetation cover

Table 2 lists the e-folding times (negative reciprocals of the eigenvalues) for EXP 1 for 3 successively smaller perturbations, denoted by P_i, $i = 1, 2, 3$. All eigenvalues are negative and real, indicating a locally stable and nonoscillatory system. The e-folding times range from 5 minutes (mode 1) to about four months (mode 6). The e-folding times of the first five modes from the second perturbation are almost identical to

Table 2: The e-folding times for EXP 1. The tangent linear matrix $A(\bar{X})$ was derived using successively smaller perturbations, indicated by P1, P2, and P3.

PERT.	MODE 1	MODE 2	MODE 3	MODE 4	MODE 5	MODE 6
P1	5.06 min	19.71 min	1.04 hr	3.15 day	11.52 day	111.93 day
P2	5.06 min	19.68 min	7.60 hr	3.30 day	11.52 day	118.72 day
P3	5.07 min	19.67 min	7.62 hr	3.30 day	11.52 day	104.85 day

those from the third perturbation, indicating convergence. The last mode shows some oscillation due to the numerical difficulty of solving for the minimum eigenvalue of a matrix with a wide range of eigenvalues; the ratio of the largest to the smallest eigenvalue exceeds four orders of magnitude.

Figure 3 shows the six normalized eigenvectors (modes) for EXP 1, corresponding to P3 in Table 2. Each panel corresponds to one mode and the bars denote the magnitude of the elements. Each element is associated with one of the six prognostic variables or state perturbations. Our discussion will be qualitative, focusing on the dominant variables for each mode. While a moderate change of the scaling values would affect the quantitative appearance of Fig. 3, it would not affect the qualitative features.

The first mode shows that a perturbation in the surface vapor pressure e_a alone will decay quickly, with a 5-minute e-folding time. The second mode indicates the coupling of T_c with e_a. For this mode, a high surface temperature provides more energy for surface evaporation, and increases the moisture-holding capacity of the surface air. The near-surface air moisture gradient then increases, which stimulates more evaporation from the ground. This mode has a 20-minute e-folding time scale. The third mode shows a relatively weak negative coupling between the soil moisture in the top two layers. The fourth and sixth modes depict the coupling between the soil moisture in the three layers. The soil moisture transfer in the three layers exhibits two distinctive time scales. The fourth mode, representing soil moisture transfer from the third layer to the upper two layers (or the reverse), has about a 3-day e-folding time. The sixth mode, representing moisture transfer throughout the entire soil column, has a time scale of about 3 months. The fifth mode primarily isolates T_d with a 12-day e-folding time.

Table 3 lists the e-folding times for each mode of EXP 2. Again all eigenvalues are negative and real. The six eigenvectors corresponding to the fifth perturbations $P5$ (Fig. 4) are similar to those of EXP 1. The e-folding times of EXP 2 are comparable to those of EXP 1. However, the third and sixth modes, which represent soil moisture transfer from the top soil layer and throughout the whole soil column respectively, have much shorter time scales. The reduction in time scales of these two modes corresponds to the lower basic state soil wetness (Table 1) of EXP 2 compared with EXP 1.

Table 3: As in Table 2 but for EXP 2.

PERT.	MODE 1	MODE 2	MODE 3	MODE 4	MODE 5	MODE 6
P1	5.03 min	16.21 min	4.49 hr	3.43 day	11.39 day	47.77 day
P2	5.01 min	16.19 min	4.56 hr	3.56 day	11.41 day	51.65 day
P3	5.01 min	16.86 min	4.61 hr	3.59 day	11.45 day	52.87 day
P4	5.02 min	16.86 min	4.61 hr	3.59 day	11.45 day	48.92 day
P5	5.00 min	16.88 min	4.61 hr	3.59 day	11.46 day	58.49 day

b. Eigenanalysis for the two experiments without vegetation cover

Table 4 and Fig. 5 show the eigenvalues and eigenvectors for EXP 3, which has the same basic state as EXP 1 but with bare soil. The e-folding times of EXP 3 are significantly shorter than those of both EXP 1 and EXP 2. The first three modes have time scales on the order of minutes. There are no intermediate modes with e-folding times between one hour and 10 days. The longest time scale is reduced to about a month.

Unlike EXP 1 and EXP 2, the first eigenvector of EXP 3 (Figure 5) represents the soil moisture transfer between the first two adjacent soil layers. The e-folding time of this mode is about 4 minutes, which is much shorter than that of the corresponding mode in EXP 1 and EXP 2 (third mode). This reduction in time scale results from two factors. First, bare soil has no evapotranspiration, so soil moisture evaporates directly from the surface. Second, the soil depth of the first two layers is shallow (see Table 1), so moisture transfer is fast. The second mode isolates e_a with a 5-minute time scale, which is similar to the first mode

Table 4: Similar to Table 2 except for EXP 3.

PERT.	MODE 1	MODE 2	MODE 3	MODE 4	MODE 5	MODE 6
P1	4.47 min	4.96 min	28.08 min	57.08 min	11.87 day	23.46 day
P2	4.15 min	4.96 min	28.04 min	59.25 min	11.87 day	24.49 day
P3	3.91 min	4.96 min	28.03 min	1.00 hr	11.87 day	24.57 day
P4	3.73 min	4.96 min	28.03 min	1.03 hr	11.87 day	26.07 day
P5	3.55 min	4.96 min	28.03 min	1.08 hr	11.82 day	21.47 day
P6	3.55 min	4.96 min	28.03 min	1.08 hr	11.87 day	30.04 day

Table 5: Similar to Table 2 except for EXP 4.

PERT.	MODE 1	MODE 2	MODE 3	MODE 4	MODE 5	MODE 6
P1	4.13 min	5.25 min	25.24 min	1.45 hr	3.15 day	13.03 day
P2	4.30 min	5.25 min	25.19 min	1.46 hr	3.41 day	13.06 day
P3	4.34 min	5.25 min	25.19 min	1.46 hr	3.50 day	13.07 day
P4	4.35 min	5.25 min	25.18 min	1.46 hr	3.50 day	13.06 day
P5	4.35 min	5.25 min	25.18 min	1.46 hr	3.48 day	13.05 day
P6	4.35 min	5.25 min	25.18 min	1.46 hr	3.60 day	13.12 day
P7	4.35 min	5.24 min	25.20 min	1.46 hr	3.56 day	13.06 day

of the two previous experiments. The third mode shows the positive coupling between T_c and ϵ_a with a 28-minute e-folding time, which is relatively long compared with the corresponding mode in EXP 1 and EXP 2 (second mode). Once again, the fourth and sixth modes depict two different soil moisture transfer processes, but now with shorter timescales. The fourth mode, with a one hour time scale, shows a negative relationship between the soil moisture in the upper two layers and that of the third layer. The sixth mode, with about a one month time scale, depicts transfer of moisture throughout the entire soil column. The fifth mode that primarily isolated T_d in EXP 1 and EXP 2 now also includes components of moisture exhibiting a similar time scale. Its e-folding time is comparable to that in EXP 1 and EXP 2.

Table 5 lists the e-folding times for EXP 4. They are comparable with those of EXP 3, except that of mode 5 (around 3 days), which represents soil moisture transfer throughout the entire soil column (compared with mode 6 of EXP 3, around 30 days). Figure 6 displays the eigenvectors for EXP 4. Similarly to EXP 3, the first eigenvector depicts a negative coupling between the soil moisture in the first

two soil layers. However, e_a appears as a dominant variable in this mode. The second mode again isolates e_a. The third mode shows once more the coupling between T_c and e_a, with an e-folding time of 25 minutes. Modes 4 and 5 represent significant moisture transfer among the model layers. The time scale of mode 5 is reduced to about 3.5 days which is probably related to the smaller initial soil wetness used in EXP 4. Again, there is a mode isolating T_d (last mode) with about a 13-day time scale, similar to mode 5 of EXP 3.

c. Summary of the four experiments

The results from all four experiments show common features even though different basic states and land covers were used. Tables 6 and 7 summarize the modes and associated physical processes. The e-folding times range widely in all experiments indicating clear different characteristic time scales of these land surface processes. There are several distinctive modes including those isolating e_a, T_d, soil moisture transfer and coupling between T_c and e_a.

The two different basic states generally do not produce large changes in eigenvalues (EXP 1 versus EXP 2, EXP 3 versus EXP 4). However, the mode that represents soil moisture transfer in the entire soil column shows a much shorter time scale when the basic state of 13Z monthly mean for June is used. This suggests that higher basic state surface temperature and vapor pressure and lower soil wetness causes a soil moisture perturbation decaying more quickly throughout the soil column.

The eigenvectors of EXP 1 and EXP 2 are also similar, as are those of EXP 3 and EXP 4. However, the eigenvectors change significantly depending on whether or not there is vegetation cover.

The impact of vegetation is clear. In bare soil (EXP 3, EXP 4), the three modes representing soil moisture transfer have much shorter e-folding times compared with those obtained when there is vegetation covering (EXP 1, EXP 2). The soil moisture perturbation in the first two layers is also coupled.

The mode isolating the T_d perturbation has a consistent e-folding time across the four experiments. The

reason is explained by examining the linearized T_d prognostic equation (2). The solution of the linearized perturbation equation shows that the e-folding time of T_d perturbation is determined mainly by the soil heat capacity and the depth of of soil layer where the temperature varies slowly and does not have diurnal variation. In the Mosaic LSM, these parameters are the same for grass and bare soil.

Table 6: Description of the eigenmodes derived from EXP 1 and EXP 2. The e-folding times for EXP 2 are given in parentheses.

Mode Description	Mode Order	e-folding Time
Dominant e_a perturbation	Mode 1	5.07 (5.00)min
Coupling between T_c and e_a	Mode 2	19.67 (16.88) min
Dominant W_1 perturbation	Mode 3	7.62 (4.61) hr
Coupling of soil moisture in the three soil layers. Moisture perturbation in the deep layer has the opposite sign of that in the upper two layers.	Mode 4	3.30 (3.59) day
Dominant T_d perturbation	Mode 5	11.52 (11.46) day
Coupling of soil moisture. Signs of the soil moisture perturbations are the same in the three layers.	Mode 6	104.85 (58.49) day

Table 7: Description of the eigenmodes derived from EXP 3 and EXP 4. The e-folding times and the different mode orders for EXP 4 are given in parentheses.

Mode Description	Mode Order	e-folding Time
Dominant e_a perturbation	Mode 1	4.96 (5.24)min
Coupling of soil moisture between the upper two soil layers. In EXP 4, this coupling is associated with e_a perturbation	Mode 2	3.55 (4.35) min
Coupling between T_c and e_a perturbation	Mode 3	28.03 (25.20) min
Coupling of soil moisture in the three soil layers. Moisture perturbation in the deep layer has the opposite sign of that in the upper two layers.	Mode 4	1.08 (1.46) hr
Dominant T_d perturbation	Mode 5 (Mode 6)	11.87 (13.06) days
Coupling of soil moisture. Signs of the soil moisture perturbations are the same in the three layers.	Mode 6 (Mode 5)	30.04 (3.56) day

5. Eigenanalysis of soil moisture dynamic subsystem

As shown above, the modes representing the evolution of soil moisture perturbations have relatively long time scales. These modes are important because they retain the initial soil moisture error with the model

integrations. These modes are also weakly coupled with other land surface state variables as suggested by the eigenvector patterns shown above. We therefore derive a soil moisture subsystem by isolating soil moisture variables to further examine soil moisture dynamics. This subsystem consists of equations (5), (6), and (7). The tangent linear matrix was obtained analytically. We then evaluate the tangent linear matrices using basic states and land covering conditions described in Section 3b. The scaling magnitudes for soil moisture are the same as used in section 3. The details of deriving this subsystem are given in the Appendix.

a. Eigenvalues and eigenvectors

The tangent linear matrices for the soil moisture subsystem are similar to the corresponding submatrix of the full system. The magnitudes generally differ from that of the full system by less than 1%. Again, all eigenvalues are negative and real. Table 8 lists the e-folding times for the four experiments. The values of the first two modes are comparable with those derived from the 6-equation system (see Table 2-Table 5). The modes of EXP 1 and 2 again exhibit longer time scales than those of EXP 3 and 4. However, the e-folding time of the last mode differs considerably from the previous experiments. This large difference is likely related to the lack of the soil moisture coupling with other state variables in this subsystem.

Figure 7 illustrates the three normalized eigenvectors derived from this subsystem with the conditions of EXP 1. The first mode mainly represents the evolution of the surface layer soil moisture perturbation. The second mode shows the soil moisture transfer from the top two layers to the deep layer during the decaying of th esoil moisture perturbations. The third mode represents the soil moisture extraction in the entire soil column. As before, the third mode has the longest time scale. Figure 8 shows that the three eigenvectors with EXP 2 conditions are comparable to that of EXP 1. Figures 9 and 10 display the three eigenvectors with the conditions used in EXP 3 and 4. The eigenvectors of all four experiments derived from the subsystem are similar to the respective eigenvectors derived from the 6-equation system. This

indicates that the behavior of soil moisture perturbation in the full TLM can be approximated by that of a TLM from a simplified sub-system.

Table 8: The e-folding times derived from the TLM of the soil dynamic subsystem for the four experiments.

EXP. LABEL	MODE 1	MODE 2	MODE 3
EXP 1	7.46 hr	3.29 day	93.79 day
EXP 2	9.50 hr	3.89 day	75.57 day
EXP 3	3.57 min	1.09 hr	17.70 day
EXP 4	4.34 min	1.63 hr	12.37 day

b. Key parameters

We further simplify this soil moisture dynamic subsystem to get explicit dependencies on key parameters. We first rewrite the equation (A1) (see Appendix) including only the dominant terms that are evaluated with the basic state values described in Section 3:

$$\frac{dW'}{dt} = BW' \approx \left(\hat{b}_{i,j}\right) W', \tag{15}$$

where $\hat{b}_{ij}$ denotes a dominant term in the equation (A1), and W' is the soil moisture perturbation (see Appendix). Tables 9 and 10 list these dominant terms (with signs) for EXP 1 and EXP 3, respectively. The dominant terms for EXP 2 and EXP 4 are similar but with slight changes. For both grass and bare soil land conditions, the terms representing moisture flux and the impact of soil moisture on surface evaporation are dominant, whereas the influence of soil moisture on evapotranspiration is less important. Soil physical parameters and soil layer depth are the key parameters as shown below. Note that W_i denotes the mean state of soil moisture here.

For convenience, we list the notations used below and in the Appendix.

K_i, h_i, ψ_i: soil hydraulic conductivity, hydraulic head, and soil moisture potential in layer ith respectively

b: a soil parameter related to soil pore size distribution index

$\Delta Z_{i,j}$: mean depth between the ith and jth soil layer

Table 9: $\hat{b}_{i,j}$, the dominant terms of the tangent linear matrix of the soil dynamical system, equation (15), with a grass land cover condition (EXP 1).

$\frac{dW'_i}{dt}$	$\hat{b}_{i,1}$	$\hat{b}_{i,2}$	$\hat{b}_{i,3}$
i=1	$\frac{\rho_w K_2 b \psi_1}{\Delta Z_{1,2} W_1} - \frac{12 E_{bs}^2 r^{-2}}{C_1 W_1}$	$-\frac{\rho_w K_2 b \psi_2}{\Delta Z_{1,2} W_2} - Q_{1,2} \frac{(2b+3)}{W_2}$	0
i=2	$\frac{-\rho_w K_2 b \psi_1}{\Delta Z_{1,2} W_1}$	$\frac{\rho_w K_2 b \psi_2}{\Delta Z_{1,2} W_2} + \frac{\rho_w K_3 b \psi_2}{\Delta Z_{2,3} W_2} + Q_{1,2} \frac{2b+3}{W_2}$	$-\frac{2b+3}{W_3} Q_{2,3} - \frac{\rho_w K_3 \psi_3 b}{\Delta Z_{2,3} W_3}$
i=3	0	$-\frac{\rho_w K_3 \psi_2 b}{\Delta Z_{2,3} W_2}$	$\frac{2b+3}{W_3} Q_{2,3} + \frac{\rho_w K_3 \psi_3 b}{\Delta Z_{2,3} W_3} - \frac{2b+3}{W_3} Q_{3,\infty}$

r_{bs}: resistance to bare soil evaporation

$q_s(T_c)$: saturated specific humidity at T_c

q_a: air specific humidity

r_{surf}: resistance provided by the soil itself to bare soil evaporation

r_{sca}: vegetation specific constant

f_{hum}: relative humidity factor on the resistance to bare soil evaporation.

E_T: total evapotranspiration

r_c: Canopy resistance to transpiration

$r_{c-unstress}$: unstressed canopy resistance to transpiration, independent of soil wetness

$F(VPD)$ and $F(T)$: factors by which canopy resistance increases due to temperature and vapor pressure deficit (VPD) stress respectively, independent of soil moisture.

$F(\psi_l)$: factor by which canopy resistance increase due to leaf water potential stress, dependent on soil moisture

ψ_r: soil moisture potential in the root zone

r_{plant}, ψ_1^c, ψ_2^c, r_{s1}, r_{s2}: prescribed physical parameters in the Mosaic LSM

E_T^*: an estimate of evapotranspiration

K_{avg}: averaged hydraulic conductivity in the root zone, dependent on soil moisture

C_1 and r^{-2}: see the appendix for explanation.

Table 10: $\hat{b}_{i,j}$, dominant terms in the tangent linear matrix of the soil dynamical system, equation (15), with a bare soil land cover condition (EXP 3).

$\frac{dW'_i}{dt}$	$\hat{b}_{i,1}$	$\hat{b}_{i,2}$	$\hat{b}_{i,3}$
i=1	$\frac{\rho_w K_2 b\psi_1}{\Delta Z_{1,2} W_1}$	$-\frac{2b+3}{W_2}Q_{1,2} - \frac{\rho_w K_2 b\psi_2}{\Delta Z_{1,2} W_2}$	0
i=2	$-\frac{\rho_w K_2 b\psi_1}{\Delta Z_{1,2} W_1}$	$\frac{2b+3}{W_2}Q_{1,2} + \frac{\rho_w K_2 b\psi_2}{\Delta Z_{1,2} W_2} + \frac{\rho_w K_3 b\psi_2}{\Delta Z_{2,3} W_2}$	$-\frac{(2b+3)}{W_3}Q_{2,3} - \frac{\rho_w K_3 \psi_3 b}{\Delta Z_{2,3} W_3}$
i=3	0	$-\frac{\rho_w K_3 \psi_2 b}{\Delta Z_{2,3} W_2}$	$\frac{(2b+3)}{W_3}Q_{2,3} + \frac{\rho_w K_3 \psi_3 b}{\Delta Z_{2,3} W_3}$

We discuss the solution of equation (15) under two simplifying assumptions.

Assumption 1: Assume that the soil moisture perturbation in the top layer (w'_1) is decoupled from the other two variables. This simplification holds in EXP 1 and 2 (shown by the first eigenvector patterns in Figs 7 and 8). Equation (15) then becomes:

$$\frac{dw'_1}{dt} \approx \hat{b}_{1,1} w'_1, \tag{16}$$

and the solution is

$$w'_1(t) = w'_1(0) exp(\hat{b}_{1,1} t). \tag{17}$$

From Tables 9, we see that the e-folding time, $\frac{-1}{\hat{b}_{1,1}}$, has two components. The first component is proportional to $\Delta Z_{1,2}$ and W_1, and inversely proportional to soil conductivity and soil moisture potential of layers 1 and 2, and soil constant b. For EXP 3 with bare soil, $\hat{b}_{1,1}$ has only one term.

Assumption 2: Assume that the deep soil moisture perturbation w'_3 is decoupled from the other two soil moisture variables. In fact, w'_3 is a dominant variable in the third eigenvector for the all four experiments (Fig 7 to Fig. 10). Then we have a form similar to (16) holds for w'_3. The e-folding time $\frac{-1}{\hat{b}_{3,3}}$ for w'_3 increases with $\Delta Z_{2,3}$ and W_3, and decreases with soil conductivity and soil moisture potential of the third layer, and soil constant b. For the case with grass, the moisture flux leaving the column also plays role.

The soil moisture perturbation at the second layer w'_2 is always tightly coupled with either w'_1 or w'_3 with intermediate time scale compared to the above two isolated modes. The experiments show that the

e-folding time of the coupling mode increases with the mean depth between the layers one and two, and decreases with soil physical parameters listed above.

Table 11 summarizes these relationships between the e-folding time and key parameters and mean state derived from the simplified situations. Of these key parameters, the mean depth of the adjacent two soil layers, $\Delta Z_{1,2}$ and $\Delta Z_{2,3}$, mainly accounts for the large differences in the e-folding time between the experiments with vegetation and without vegetation. This is because all the other key parameters are the same for grass and bare soil conditions in the Mosaic LSM. These results agree qualitatively with previous studies (Yang et al. 1995; Yang et al., 1994).

Table 11: General relationships between the e-folding times and dominant items of the tangent linear matrix for soil moisture subsystem.

Magnitude of e-folding time decreases with:	soil hydraulic conductivity: K_1,K_2, K_3 soil hydraulic potential: ψ_1, ψ_2, ψ_3 soil constant: b
Magnitude of e-folding time increases with:	basic state of soil moisture: W_1, W_2,W_3 mean depth of soil layer: $\Delta Z_{1,2}$, $\Delta Z_{2,3}$

6. Summary and discussion

The TLM eigenanalysis efficiently computes the characteristic time scales and structure of the model's land surface state perturbations. It effectively synthesizes the impact of different basic state and vegetation conditions on the evolution of initial state errors. An understanding of these features is important for assimilating land surface data into models and for improving the physical parameterizations in the land surface schemes. It also provides additional information about the natural variability in a Mosaic LSM.

The main results are summarized as follows:

(1) The Mosaic LSM exhibits a wide range of internal variability. The e-folding times of the different

modes range from a few minutes to about 3 months. Modes representing the evolution of perturbations in surface temperature and surface moisture exhibit short time scales. The modes representing the evolution of soil moisture perturbations within the whole soil column exhibit longer time scales. The mode representing the deep soil temperature (T_d) perturbation is weakly coupled to the other land surface variables and has a consistent e-folding time across the experiments.

(2) The time scales depend significantly upon vegetation parameters, soil parameters, and basic state conditions. The modes representing the behavior of soil moisture perturbations have significantly longer time scales when vegetated. The influence of two different basic states is relatively small because the two states used here are not significantly different. However, warm surface temperature and high surface air moisture tend to shorten the e-folding times.

(3) For the simplified soil moisture dynamic subsystem, the terms representing moisture flux and the effect of soil moisture on surface evaporation are important. Whereas the effect of soil moisture on evapotranspiration is not significant. Note these results are with respect to the forcing condition used. In particular, soil moisture is not dry. The key parameters determining the e-folding time include: the mean depth of soil layer, soil hydraulic conductivity and potential, soil parameter b, and mean soil moisture. Deeper and wetter soils have longer time scales. Soils with high soil constant b and high soil hydraulic conductivity and potential tend to have short time scales.

(4) The experiments suggest that the Mosaic LSM is stable with respect to the basic states used. Any initial perturbation, or initial error, will decay with time. The constraints based on physical principles in the Mosaic LSM appear to prevent instabilities of the land surface state perturbations.

The results highlights the importance of accurate initial soil moisture and deep soil temperature information in land surface data assimilation. The initial errors in soil moisture and deep soil temperature decay slowly. Therefore, emphasis should be placed on obtaining highly accurate data for these variables.

The results also show the significant dependence of the time scale on vegetation condition and soil physical parameters. Currently there is uncertainty in these prescribed parameters. However, it is very promising that the use of Satellite data from advanced instruments, such as Moderate-Resolution Imaging Spectroradiometer (MODIS) on Earth Observing System (EOS), will improve global estimates of soil moisture and those parameters.

We must be careful when generalizing the results obtained in this study. First, the results were obtained with respect to two sets of basic state and vegetation conditions. For other regions with different atmospheric and vegetation conditions, eigenvalues and eigenvectors may be different. Second, we chose perturbation magnitudes in a way that ensures the perturbed state stays in the same local continuous domain as the basic state. In reality, the perturbed state may evolved towards a different domain. In this case the linear approximation around the basic state does not hold. A thorough discussion regarding this issue is given by Errico (1997). Finally, the selection of perturbation and scaling magnitudes remains an open question. The perturbation magnitudes used in this study were empirically derived based on standard deviation from the control runs. The chosen perterbation magnitudes are comparable to measurement uncertainty in these fields, but may change for different land surface regimes.

Acknowledgments:

The authors would like to thank Drs. Mahfouf and Y. Xue for providing the HAPEX Mobilhy data. We also thank Dr. R. Koster for providing the Mosaic LSM and for helpful discussions. This work was supported by the NASA Interdisciplinary Science grant on four-dimensional data assimilation.

Appendix: Linearizing the soil moisture dynamic subsystem

The prognostic equations for the three soil moisture variables in the Mosaic LSM are given in equations (4), (5), and (6).

To simplify these three equations, we assume the following: (1) surface runoff rate R_s for one time step

is negligible, and (2) soil wetness is moderate, therefore f_{hum} is approximated as one (Koster and Suarez 1995).

Following the same procedure as in the Section 3a, let $W_i = \bar{W}_i + W_i'$, to get the tangent linear model for the soil moisture dynamic subsystem:

$$\frac{dW'}{dt} = BW' = (b_{i,j})\, W'. \tag{A1}$$

Here, W' is a vector consisting of the three soil moisture state perturbations, and B is the 3x3 Jacobian matrix of this soil moisture subsystem. We obtain B analytically, as follows.

The first element, $b_{1,1}$, consists of three partial derivatives:

$$b_{1,1} \equiv \frac{\partial F_1}{\partial W_1} = -\frac{\partial E_{bs}}{\partial W_1} - \frac{\partial E_{transp,1}}{\partial W_1} - \frac{\partial Q_{1,2}}{\partial W_1}. \tag{A2}$$

To derive the first term on the right side of equation (A2), the following formulae used in the Mosaic LSM are needed:

$$E_{bs} = \frac{\rho(q_s(T_c) - q_a)}{r_{bs}} = \frac{C_1}{r_{bs}}, \tag{A3}$$

$$r_{bs} = (r_{surf} + r_{sca}) f_{hum} \approx r_{surf} + r_{sca}, \tag{A4}$$

$$r_{surf} = 26 + 6\left(\frac{W_1}{W_{1-sat}}\right)^{-2}. \tag{A5}$$

Here $C_1 = \rho(q_s(T_c) - q_a)$. Taking the partial derivative of E_{bs} with respect to W_1, we have:

$$\frac{\partial E_{bs}}{\partial W_1} = C_1 \frac{\partial}{\partial W_1}\left(\frac{1}{r_{bs}}\right) = \frac{12 C_1}{(r_{bs})^2 W_1}\left(\frac{W_1}{W_{1-sat}}\right)^{-2}. \tag{A6}$$

Applying (A3) to (A6) we have:

$$\frac{\partial E_{bs}}{\partial W_1} = \frac{12 E_{bs}^2 r^{-2}}{C_1 W_1}, \tag{A6'}$$

here, $r^{-2} = \left(\frac{W_1}{W_{1-sat}}\right)^{-2}$.

To derive the second term of the right side of equation (A2), the following formulae are needed:

$$E_{transp,1} = \frac{E_T W_1}{W_1 + W_2}, \tag{A7}$$

$$E_{transp,2} = \frac{E_T W_2}{W_1 + W_2}, \tag{A8}$$

$$E_T = \frac{C_1}{r_c}, \tag{A9}$$

$$r_c = r_{c-unstress} F(VPD) F(T) F(\psi_l), \tag{A10}$$

$$\frac{1}{F(\psi_l)} = \frac{\psi_r - Z - E_T^* \frac{r_{plant}+r_{soil}}{\rho_w} - \psi_2^c}{\psi_1^c - \psi_2^c}, \tag{A11}$$

$$\psi_r = \psi_s \left(\frac{W_1 + W_2}{W_{1-sat} + W_{2-sat}} \right)^{-b}, \tag{A12}$$

$$r_{soil} = r_{s1} + \left(\frac{r_{s2}}{K_{avg}} \right), \tag{A13}$$

$$K_{avg} = K_s \left(\frac{W_1 + W_2}{W_{1-sat} + W_{2-sat}} \right)^{2b+3}. \tag{A14}$$

Applying all of these formulae to the partial derivative of $E_{transp,1}$ in (A2), we have

$$\frac{\partial E_{transp,1}}{\partial W_1} = \frac{W_1}{W_1 + W_2} \frac{\partial E_T}{\partial W_1} + \frac{E_T W_2}{(W_1 + W_2)^2} = -\frac{W_1 C_1 \psi_r b}{(W_{root})^2 C_2 \psi^c} + \frac{c_1 E_T^* r_{s2} (2b+3) W_1}{C_2 \psi^c \rho_w K_{avg} (W_{root})^2} + \frac{E_{transp,2}}{W_{root}}, \tag{A15}$$

where $C_2 = r_{c-unstress} F(VPD) F(T)$, and $\psi^c = \psi_1^c - \psi_2^c$.

To derive the third term of the right hand of (A2), the following formulae are needed

$$Q_{1,2} = \rho_w K_2 \left(\frac{h_1 - h_2}{\delta Z_{1,2}} \right), \tag{A16}$$

$$\psi_i = \psi_s \left(\frac{W_i}{W_{i-sat}} \right)^{-b}. \tag{A17}$$

Here, ρ_w is the water density. The final expression is:

$$\frac{\partial Q_{1,2}}{\partial W_1} = -\frac{\rho_w K_2 b \psi_1}{\delta Z_{1,2} W_1}. \tag{A18}$$

$b_{1,1}$ consists of the sum of terms in equations (A6), (A15), and (A18).

The derivations of the other elements in B are similar. We therefore only list the final expressions for the other $b_{i,j}$.

$b_{1,2}$, the derivative of F_1 with respect to W_2, consist of two terms:

$$\frac{\partial F_1}{\partial W_2} = -\frac{\partial E_{transp,1}}{\partial W_2} - \frac{\partial Q_{1,2}}{\partial W_2}. \tag{A19}$$

The final expression of $b_{1,2}$ is:

$$\frac{\partial F_1}{\partial W_2} = \frac{W_1 C_1 \psi_r b}{W_{root}^2 C_2 \psi^c} + \frac{E_{transp,1}}{W_{root}} - \frac{Q_{1,2} 2b+3}{W_2} - \frac{\rho_w b K_2 \psi_2}{\delta Z_{1,2} W_2} - \frac{W_1 C_1 E_T^* r_{s2}(2b+3)}{W_{root}^2 C_2 \psi^c \rho_w K_{avg}}. \tag{A20}$$

$b_{1,3} = 0$, since F_1 is not a function of W_3.

$b_{2,1}$, the derivative of F_2 with respect to W_1, consists of two terms ($Q_{2,3}$ is not a function of W_1):

$$\frac{\partial F_2}{\partial W_1} = \frac{\partial Q_{1,2}}{\partial W_1} - \frac{\partial E_{transp,2}}{\partial W_1}. \tag{A21}$$

The final expression of equation (A21) is:

$$\frac{\partial F_2}{\partial W_1} = -\frac{\rho_w K_2 b \psi_1}{\delta Z_{1,2} W_1} + \frac{W_2 C_1 \psi_r b}{W_{root}^2 C_2 \psi^2} - \frac{W_2 C_1 E_T^* r_{s2}(2b+3)}{W_{root}^2 C_2 \psi^c \rho_w K_{avg}} + \frac{E_{transp,2}}{W_{root}}. \tag{A22}$$

$b_{2,2}$, the derivative of F_2 with respect to W_2, is:

$$\frac{\partial F_2}{\partial W_2} = \frac{\partial Q_{1,2}}{\partial W_2} - \frac{\partial E_{transp,2}}{\partial W_2} - \frac{\partial Q_{2,3}}{\partial W_2}. \tag{A23}$$

Here, $Q_{2,3} = \rho_w K_3 \frac{h_2 - h_3}{\delta Z_{2,3}}$, if soil wetness in the third layer is wetter than in the second layer. The final expression of equation (A23) is:

$$\frac{\partial F_2}{\partial W_2} = \frac{Q_{1,2}(2b+3)}{W_2} + \frac{\rho_w K_2 b \psi_2}{\delta Z_{1,2} W_2} + \frac{W_2 C_1 \psi_r b}{W_{root}^2 C_2 \psi^c} - \frac{E_{transp,1}}{W_{root}} + \frac{\rho_w K_3 \psi_2 b}{W_2 \delta Z_{2,3}} - \frac{C_1 E_T^* r_{s2}(2b+3) W_2}{C_2 \psi^c \rho_w K_{avg} W_{root}^2}. \tag{A24}$$

$b_{2,3}$, the expression of the derivative of F_2 with respect to W_3, is:

$$\frac{\partial F_2}{\partial W_3} = \frac{-Q_{2,3}(2b+3)}{W_3} - \frac{\rho_w b K_3 \psi_3}{\delta Z_{2,3} W_3}. \tag{A25}$$

$b_{3,1}$ is zero since F_3 is not a function of W_1.

$b_{3,2}$, the derivative of F_3 with respect to W_2, is:

$$\frac{\partial F_3}{\partial W_2} = \frac{\partial Q_{2,3}}{\partial W_2} - \frac{\partial Q_{3,\infty}}{\partial W_2}, \tag{A26}$$

where $Q_{3,\infty}$ is the moisture diffusion flux out the bottom of the lowest layer and depends on the topography. Since $Q_{3,\infty}$ is not a function of W_2, this expression can be simplified as:

$$\frac{\partial F_3}{\partial W_2} = \frac{-\rho_w K_3 \psi_2 b}{W_2 \delta Z_{2,3}}. \tag{A27}$$

Finally, $b_{3,3}$, the derivative of F_3 with respect to W_3, is:

$$\frac{\partial F_3}{\partial W_3} = \frac{Q_{2,3}(2b+3)}{W_3} + \frac{bK_3\psi_3\rho_w}{\delta Z_{2,3} W_3} - \frac{Q_{3,\infty}(2b+3)}{W_3}. \tag{A28}$$

The B matrix is evaluated with the basic state values described in the Section 3.

References

Brubaker, K.L., and D. Entekhabi, 1995: An analytic approach to modeling land-atmosphere interaction 1. Construct and equilibrium behavior. *Water Resources Research*, **3**, 619-632.

DAO, 1996: Algorithm Theoretical Basis Document Version 1.01, Data Assimilation Office, NASA Goddard Space Flight Center, Greenbelt, MD 20771. Available on the internet at **http://dao.gsfc.nasa.gov/subpages/atbd.html.**

Delworth and Manabe, 1988: The influence of potential evaporation on the variabilities of simulated soil wetness and climate. *J. Climate*, **1**, 523-547.

Delworth and Manabe, 1993: Climate variability and land-surface processes. *Advances in Water Resources*, **16**, 3-20.

Dickinson, R.E., 1984: Modeling evapotranspiration for three-dimensional global climate models. In *Climate Processes and Climate Sensitivity.* **Geophysical Monograph, 29**. American Geophysical Union, Washington, D.C. 58-72.

Entekhabi, D., 1995: Recent advances in land-atmosphere interaction research. *Reviews of Geophysics.* Supplement. 995-1003.

Errico, R.M. 1997: What is an adjoint model? *Bull. Amer. Meteor. Soc.*, **78**, 2577-2590.

Goutorbe, J.P., 1991: A critical assessment of the SAMER network accuracy. *Land surface Evaporation.* Ed. Schmugge and Andre, Springer-Verlag, 171-182.

Goutorbe, J.P. and C. Tarrieu, 1991: HAPEX-MOBILHY data base. *Land surface Evaporation.* Ed. Schmugge and Andre, Springer-Verlag, 403-410.

Henderson-Sellers, A., Z.-L. Yang, and R. E. Dickinson, 1993: The Project for Intercomparison of Land-surface Parameterization Schemes. *Bull. Am. Meteorol. Soc.*, **74**, 1335-1349.

Henderson-Sellers, A., B. Henderson-Sellers, D. Pollard, J. M. Verner, and A.J. Pitman, 1995: Applying software engineering metrics to land surface parameterization schemes. *J. Climate*, **8**, 1043-1059.

Koster, R.D, and M.J. Suarez, 1992: Modeling the land surface boundary in climate models as a composite of independent vegetation stands. *J. Geophys. Res.*, **97**, 2697-2715.

Koster, R.D, and M.J. Suarez, 1994: The components of a SVAT scheme and their effects on a GCM's hydrological cycle. *Adv. Water Resour.*, **17**, 61-78.

Koster, R.D, and M.J. Suarez, 1996: Energy and Water Balance Calculations in the Mosaic LSM. *NASA Technical Memorandum 104606*, **9**.

Sato, N., P.J. Sellers, D.A. Randall, E.K. Schneider, J. Shukla, J.L. Kinter, III, Y.-T. Hou, and E. Albertazzi, 1989: Effects of implementing the simple biosphere model in a general circulation model. *J. Atmos. Sci.*, **46**, 2757-2782.

Sellers, P.J., Y. Mintz, Y.C. Sud, and A. Dalcher, 1986: A simple biosphere model (SiB) for use within general circulation models. *J. Atmos. Sci.*, **43**, 505-531.

Xue, Y., H.G. Bastable, P. A. Dirmeyer, and P.J. Sellers, 1996a: Sensitivity of simulated surface fluxes to changes in land surface parameterization – a study using ABRACOS data. *J. Appl. Meteor.*, **35**, 386-400.

Xue, Y., F. J. Zeng, and C.A. Schlosser, 1996b: SSiB and its sensitivity to soil properties — a case study using HAPEX-Mobilhy data. *Global and Planetary Change*, **13**, 183-194.

Yang, R., J. Shukla, and P.J. Sellers, 1994: The influence of changes in vegetation type on the surface energy budget. *Advances in Atmospheric Sciences*, **11**, 139-161.

Yang, Z.L., R. E. Dickinson, A. Henderson-Sellers, and A.J. Pitman, 1995: Preliminary study of spin-up processes in land surface models with the first stage data of Project for Inter-comparison of Land Surface Parameterization Scheme Phase 1a (PILPS). *J. Geophys. Res.*, **100**, 16553-16578.

Figure captions

Fig. 1. The resistance network used for each tile in Mosaic LSM. The canopy covers 100% of the land surface; water evaporating from the bare soil moves through the canopy air space (from Koster and Suarez 1992).

Fig. 2. Monthly mean diurnal cycles averaged from the second June of a two-year Mosaic integration forced by a time series of the observed atmospheric conditions at the Caumont of Hapex-Mobilhy, France, 1986. Upper panel: surface ground water vapor pressure e_a (solid line) and near surface water vapor pressure e_{2m} (mb) (dashed solid line). Middle panel: ground temperature T_c (C^0) (solid line), deep soil temperature T_d (long dashed line), and near surface air temperature T_{2m} (short dash line). Bottom: soil wetness in the first layer W_1 (short dash line), root layer W_2 (long dash line), and the deep layer W_3 (solid line).

Fig. 3. Six normalized eigenvectors (in order of increasing time scales) derived from the TLM for EXP 1. A bar denotes the magnitude of each variable.

Fig. 4. Same as Fig. 3 but for EXP 2.

Fig. 5. Same as Fig. 3 but for EXP 3.

Fig. 6. Same as Fig. 3 but for EXP 4.

Fig. 7: Three normalized eigenvectors (in order of increasing time scales) derived from the soil dynamic subsystem with similar condition of EXP 1.

Fig. 8: Same as Fig. 7 but for EXP 2.

Fig. 9: Same as Fig. 7 but for EXP 3.

Fig. 10: Same as Fig. 7 but for EXP 4.

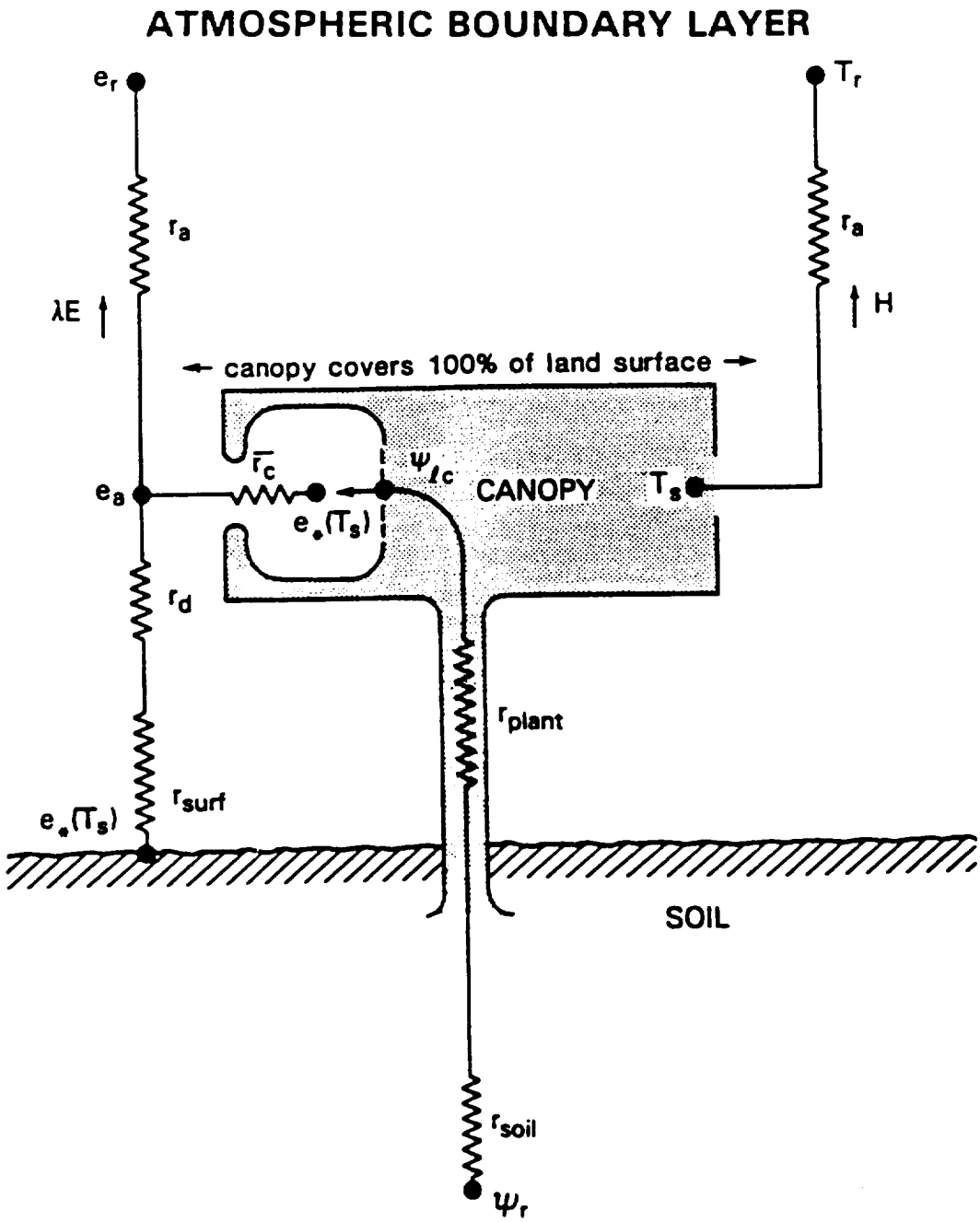
ATMOSPHERIC BOUNDARY LAYER
e_r
T_r
r_a
r_a
λE
H
canopy covers 100% of land surface
$\bar{r}_c$
ψ_{lc}
CANOPY
T_s
e_a
$e_*(T_s)$
r_d
r_{plant}
r_{surf}
$e_*(T_s)$
SOIL
r_{soil}
ψ_r

Fig. 1

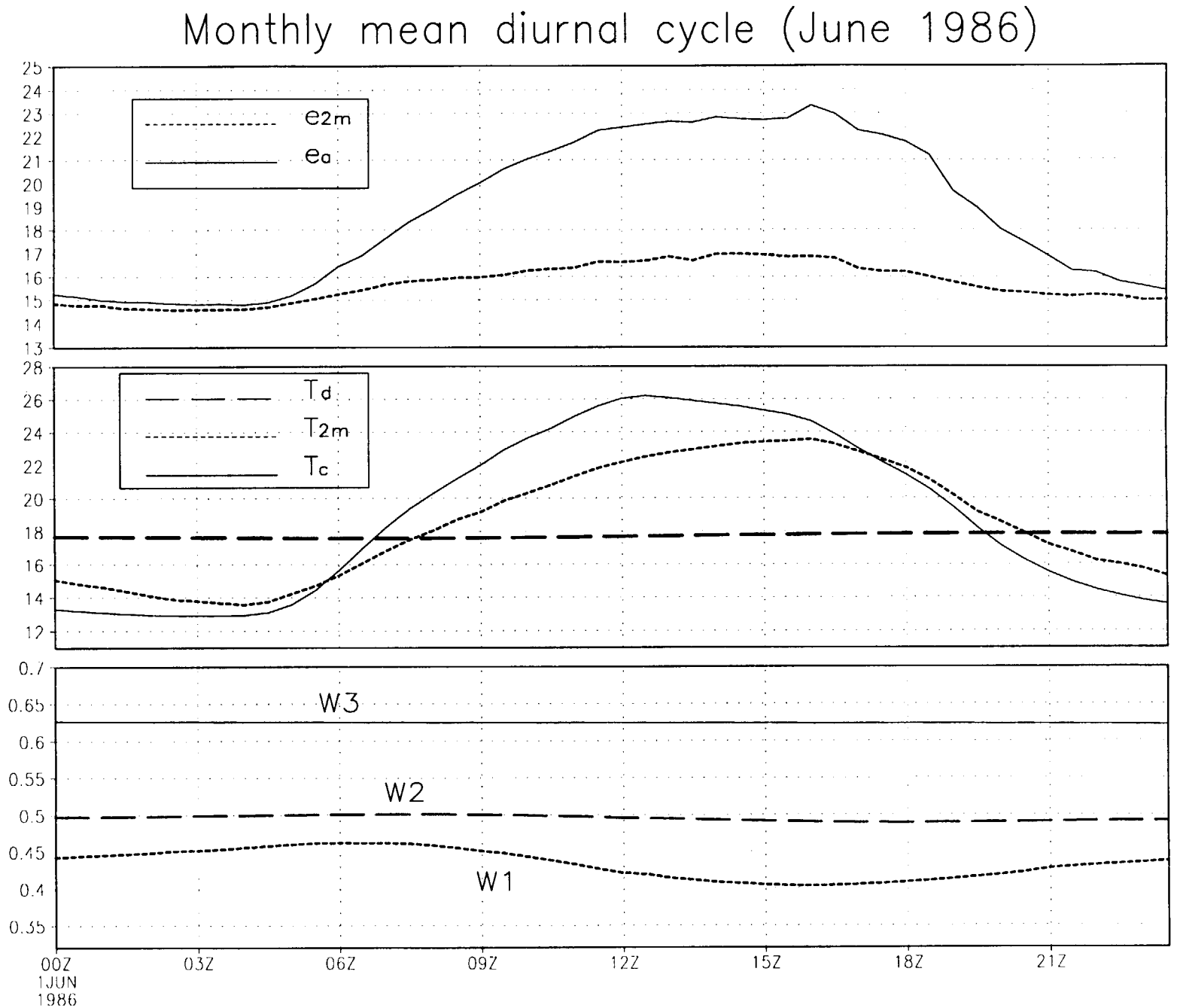
Monthly mean diurnal cycle (June 1986)
e2m
ea
Td
T2m
Tc
W3
W2
W1
00Z
1JUN
1986
03Z
06Z
09Z
12Z
15Z
18Z
21Z

Fig. 2

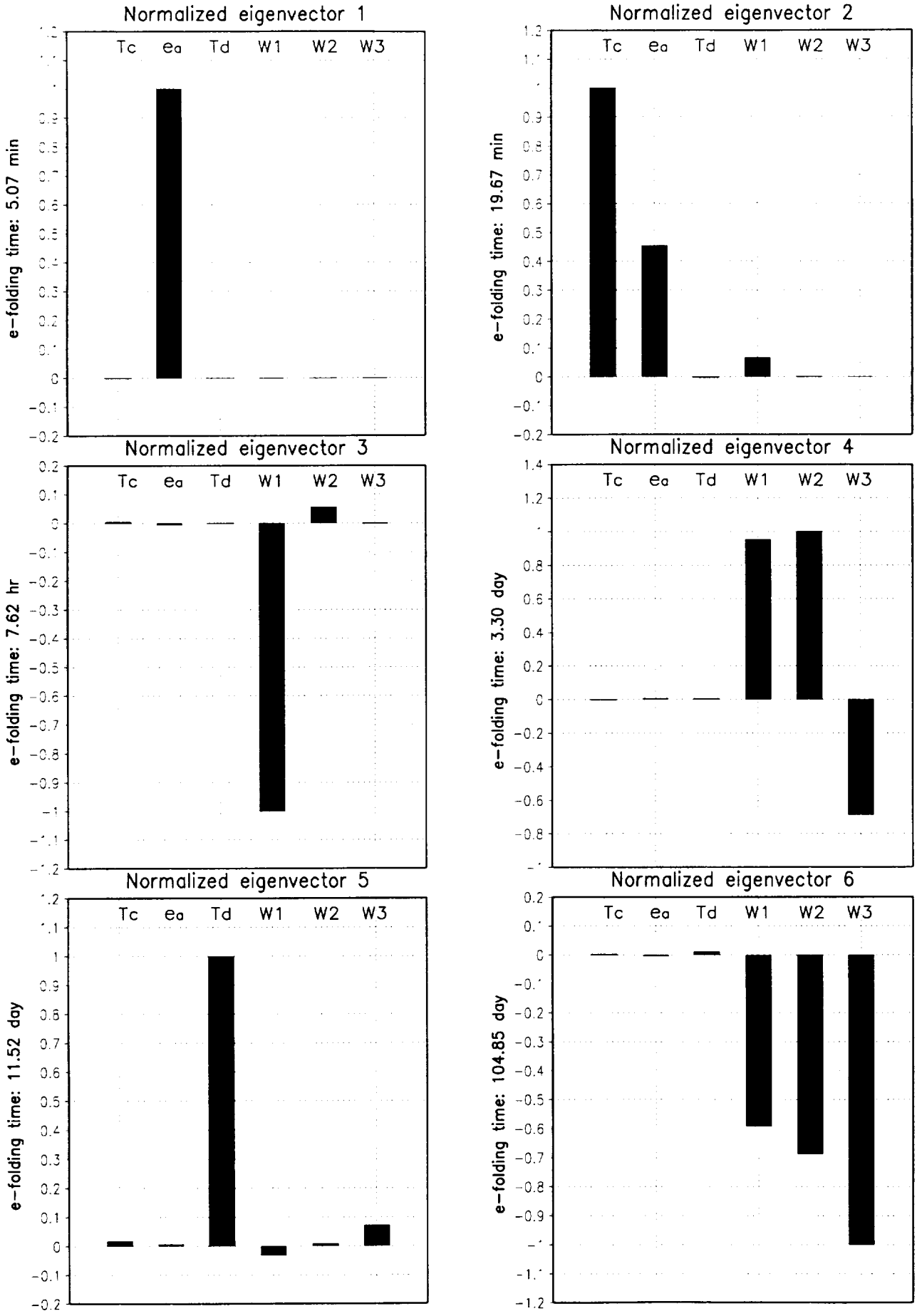
Normalized eigenvector 1
e-folding time: 5.07 min
Normalized eigenvector 2
e-folding time: 19.67 min
Normalized eigenvector 3
e-folding time: 7.62 hr
Normalized eigenvector 4
e-folding time: 3.30 day
Normalized eigenvector 5
e-folding time: 11.52 day
Normalized eigenvector 6
e-folding time: 104.85 day
Tc
ea
Td
W1
W2
W3

Fig. 3

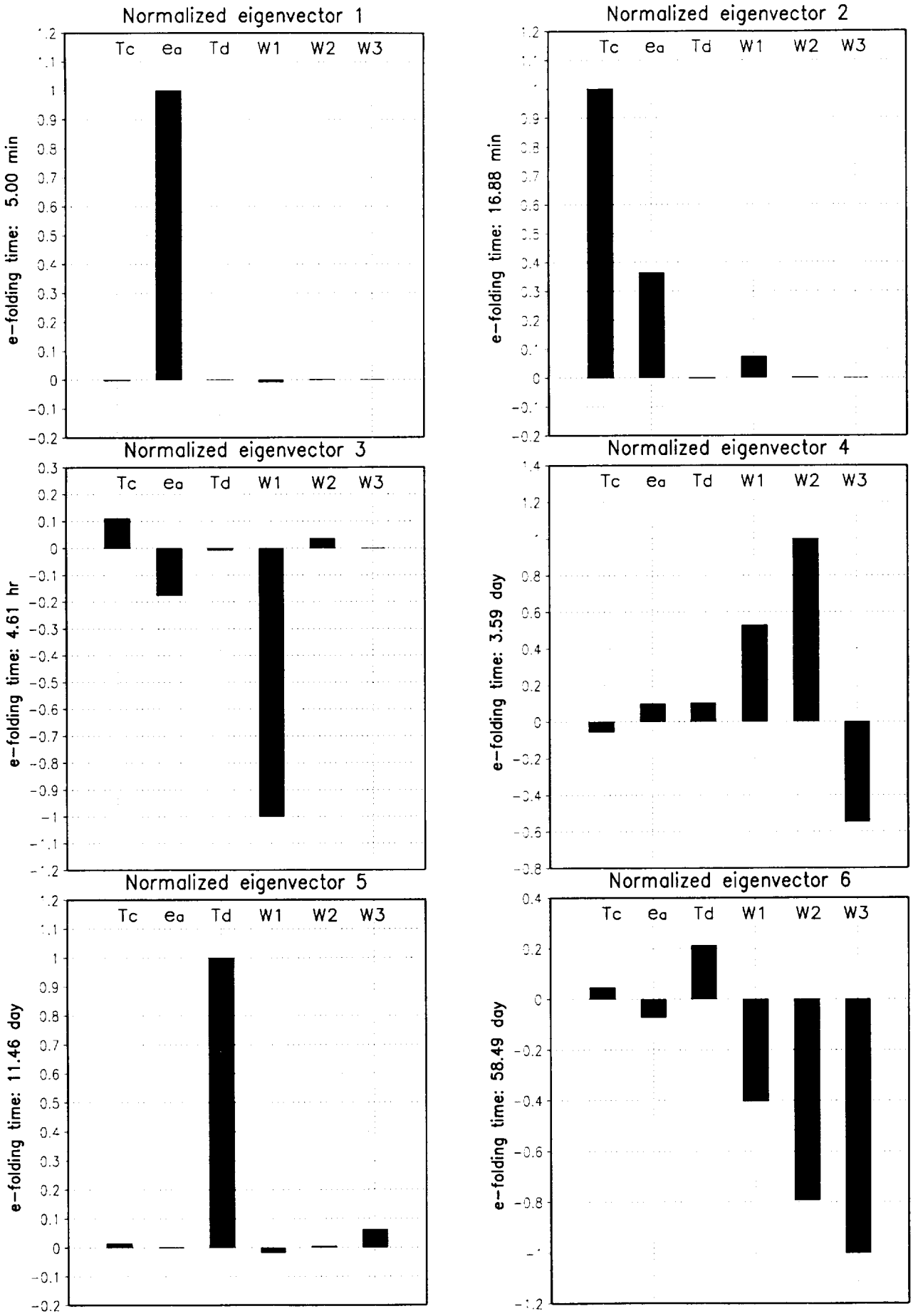
Normalized eigenvector 1
e-folding time: 5.00 min
Normalized eigenvector 2
e-folding time: 16.88 min
Normalized eigenvector 3
e-folding time: 4.61 hr
Normalized eigenvector 4
e-folding time: 3.59 day
Normalized eigenvector 5
e-folding time: 11.46 day
Normalized eigenvector 6
e-folding time: 58.49 day
Tc
ea
Td
W1
W2
W3

Fig. 4

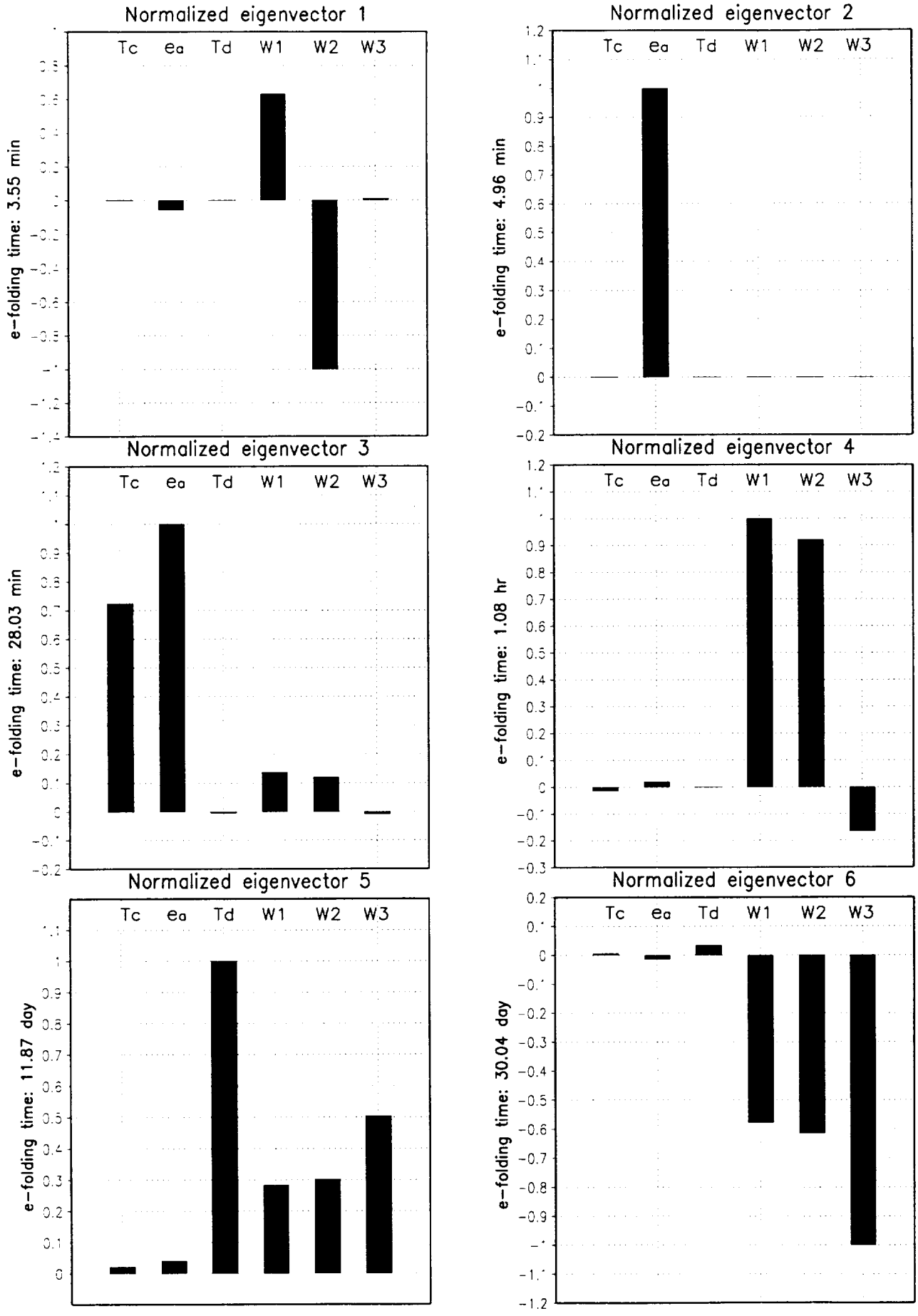
Normalized eigenvector 1
Tc
ea
Td
W1
W2
W3
e-folding time: 3.55 min
Normalized eigenvector 2
e-folding time: 4.96 min
Normalized eigenvector 3
e-folding time: 28.03 min
Normalized eigenvector 4
e-folding time: 1.08 hr
Normalized eigenvector 5
e-folding time: 11.87 day
Normalized eigenvector 6
e-folding time: 30.04 day

Fig. 5

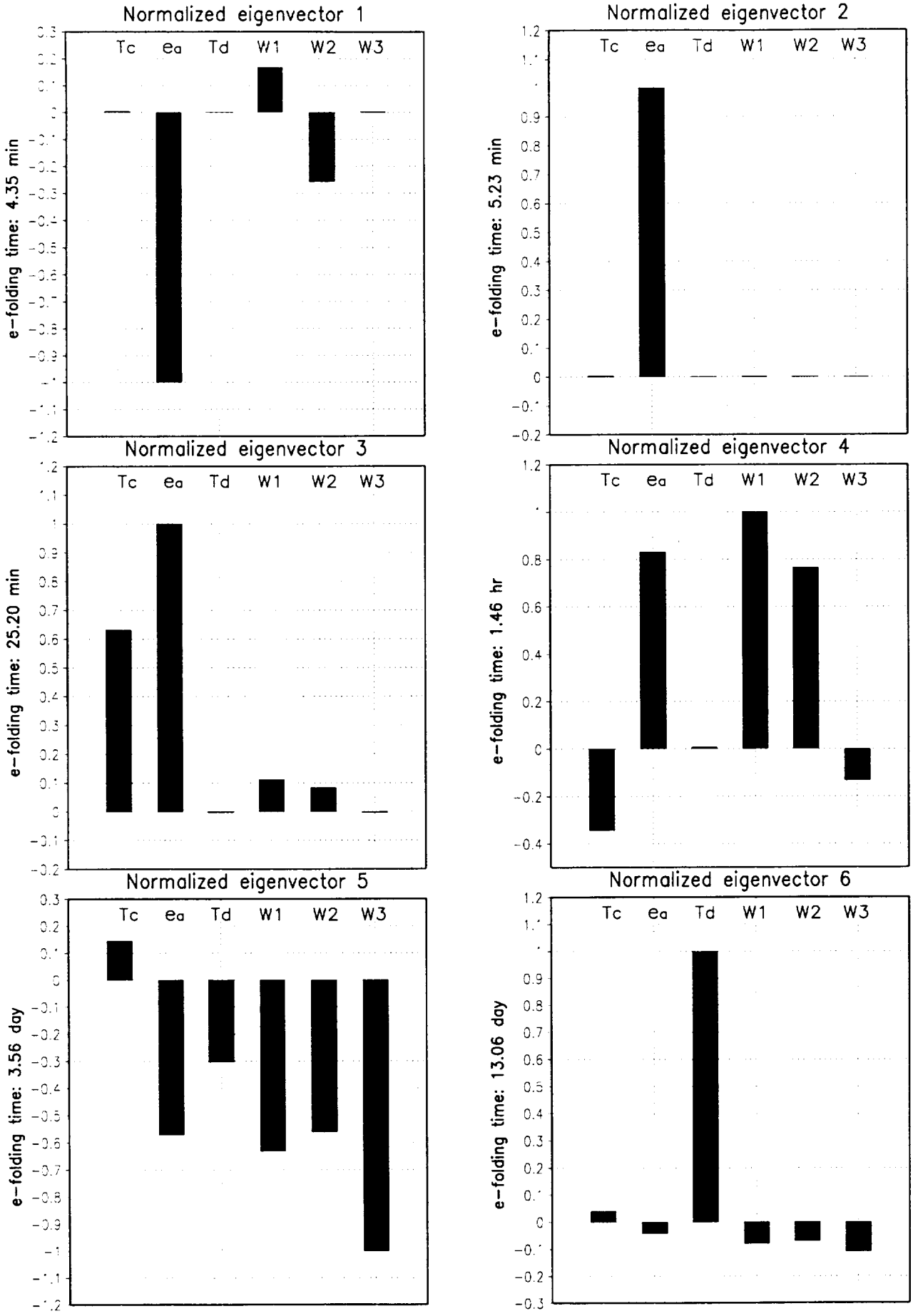
Normalized eigenvector 1
Tc ea Td W1 W2 W3
e-folding time: 4.35 min
Normalized eigenvector 2
Tc ea Td W1 W2 W3
e-folding time: 5.23 min
Normalized eigenvector 3
Tc ea Td W1 W2 W3
e-folding time: 25.20 min
Normalized eigenvector 4
Tc ea Td W1 W2 W3
e-folding time: 1.46 hr
Normalized eigenvector 5
Tc ea Td W1 W2 W3
e-folding time: 3.56 day
Normalized eigenvector 6
Tc ea Td W1 W2 W3
e-folding time: 13.06 day

Fig. 6

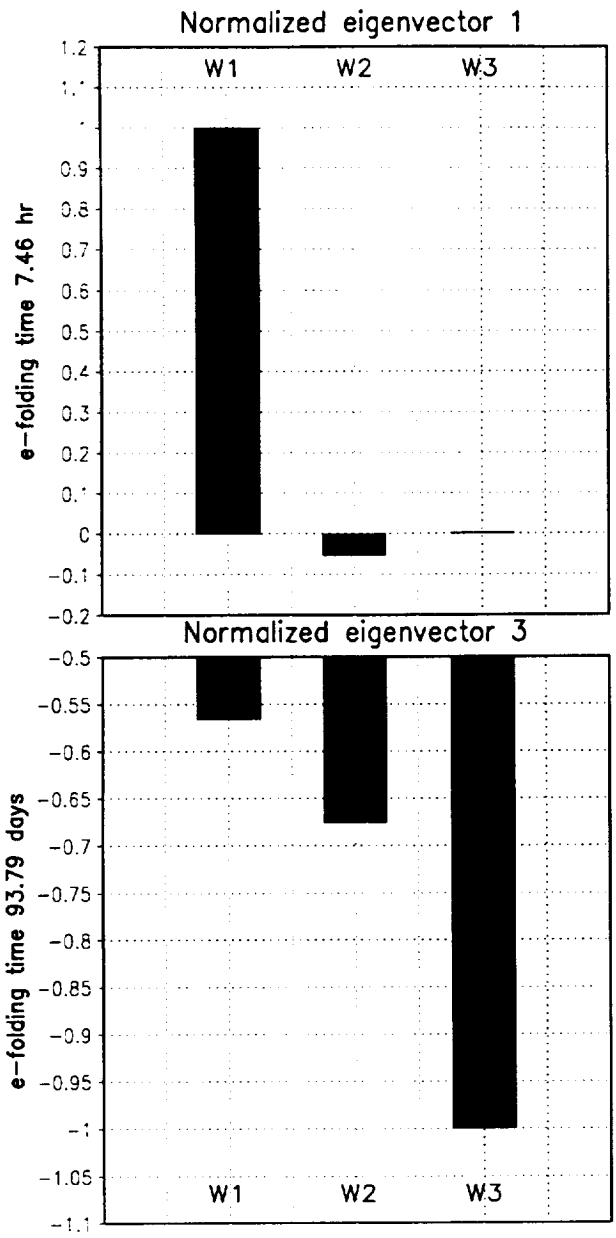
Normalized eigenvector 1
e-folding time 7.46 hr
W1
W2
W3
1.2
0.9
0.8
0.7
0.6
0.5
0.4
0.3
0.2
0
-0.1
-0.2

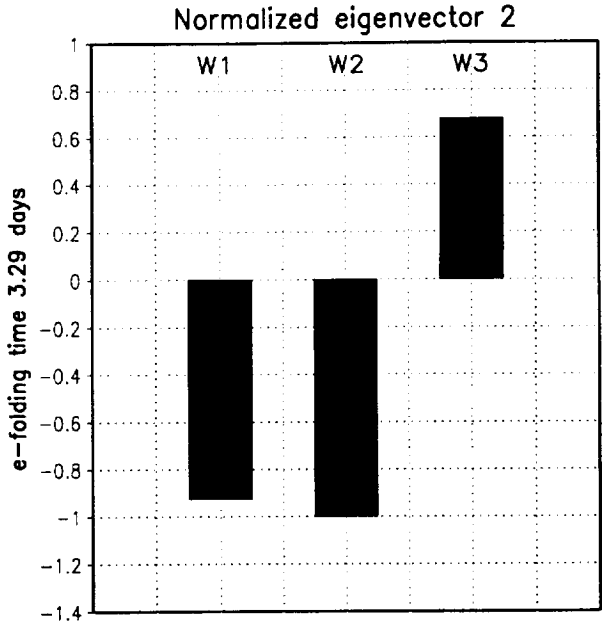
Normalized eigenvector 2
e-folding time 3.29 days
W1
W2
W3
1
0.8
0.6
0.4
0.2
0
-0.2
-0.4
-0.6
-0.8
-1
-1.2
-1.4

Normalized eigenvector 3
e-folding time 93.79 days
W1
W2
W3
-0.5
-0.55
-0.6
-0.65
-0.7
-0.75
-0.8
-0.85
-0.9
-0.95
-1
-1.05
-1.1

Fig. 7

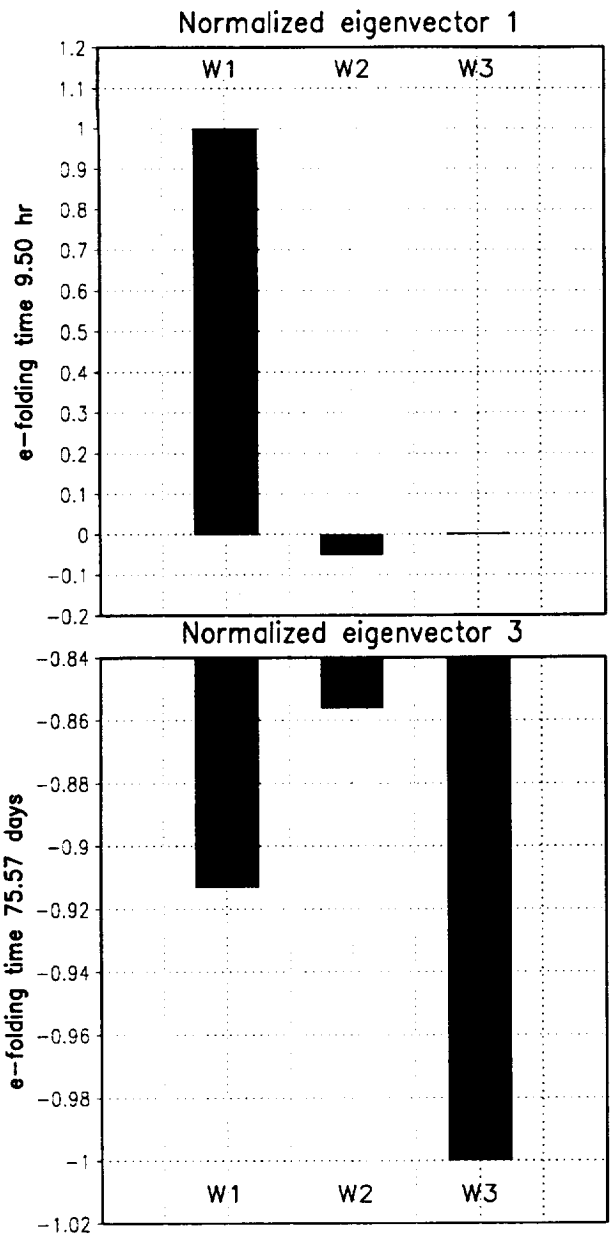
Normalized eigenvector 1
e-folding time 9.50 hr
W1
W2
W3
1.2
1.1
1
0.9
0.8
0.7
0.6
0.5
0.4
0.3
0.2
0.1
0
-0.1
-0.2
Normalized eigenvector 3
e-folding time 75.57 days
-0.84
-0.86
-0.88
-0.9
-0.92
-0.94
-0.96
-0.98
-1
-1.02
W1
W2
W3

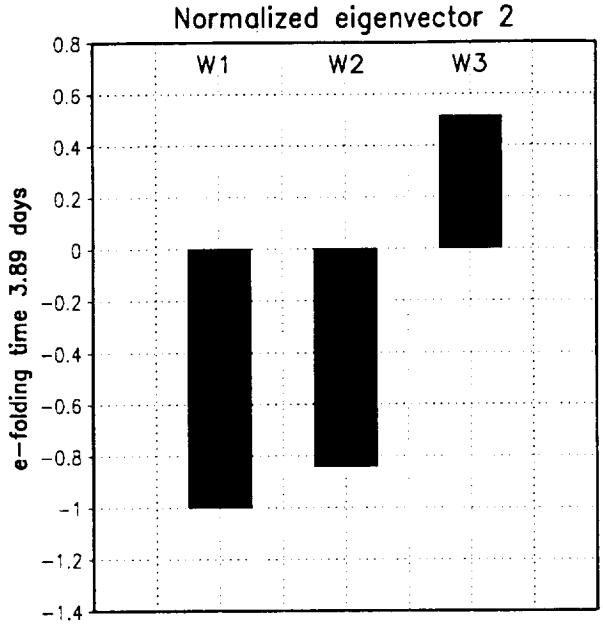
Normalized eigenvector 2
e-folding time 3.89 days
W1
W2
W3
0.8
0.6
0.4
0.2
0
-0.2
-0.4
-0.6
-0.8
-1
-1.2
-1.4

Fig. 8

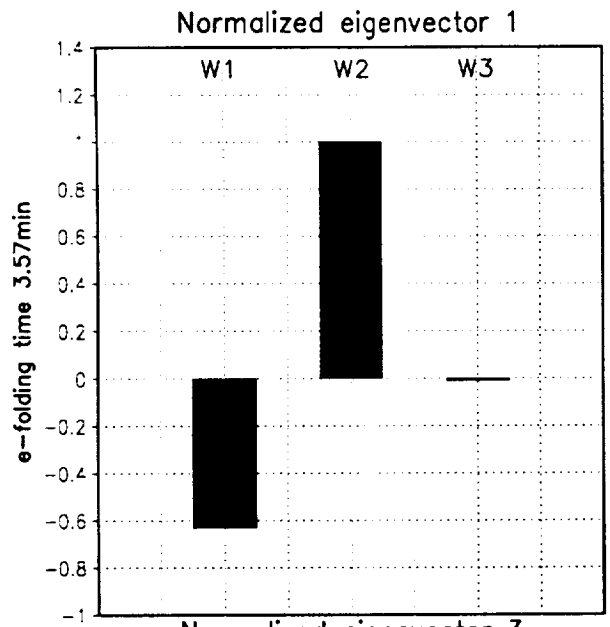
Normalized eigenvector 1
e-folding time 3.57min
W1
W2
W3
1.4
1.2
0.8
0.6
0.4
0.2
0
-0.2
-0.4
-0.6
-0.8
-1

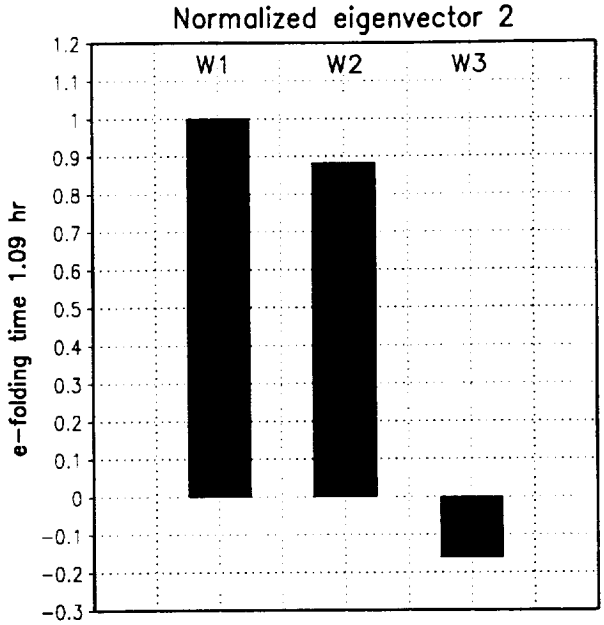
Normalized eigenvector 2
e-folding time 1.09 hr
W1
W2
W3
1.2
1.1
1
0.9
0.8
0.7
0.6
0.5
0.4
0.3
0.2
0.1
0
-0.1
-0.2
-0.3

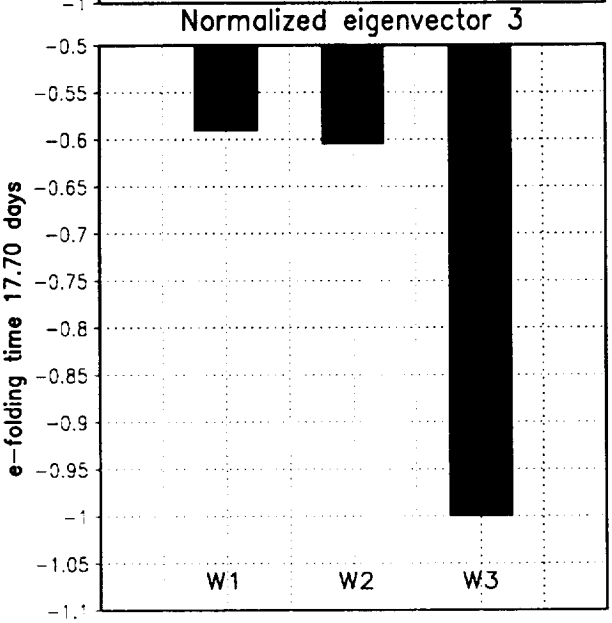
Normalized eigenvector 3
e-folding time 17.70 days
W1
W2
W3
-0.5
-0.55
-0.6
-0.65
-0.7
-0.75
-0.8
-0.85
-0.9
-0.95
-1
-1.05

Fig. 9

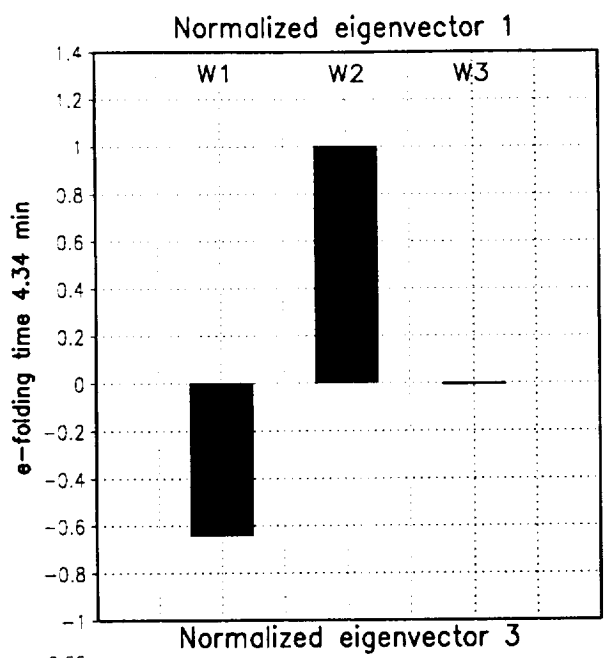
Normalized eigenvector 1
e-folding time 4.34 min
W1
W2
W3
1.4
1.2
1
0.8
0.6
0.4
0.2
0
-0.2
-0.4
-0.6
-0.8
-1

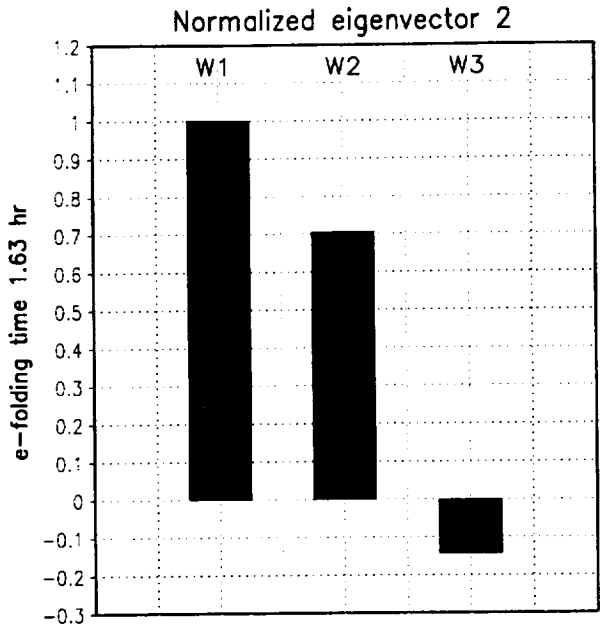
Normalized eigenvector 2
e-folding time 1.63 hr
W1
W2
W3
1.2
1.1
1
0.9
0.8
0.7
0.6
0.5
0.4
0.3
0.2
0.1
0
-0.1
-0.2
-0.3

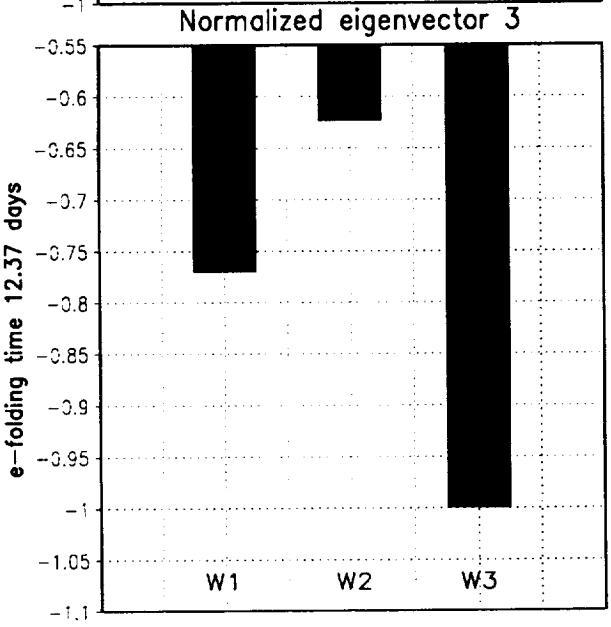
Normalized eigenvector 3
e-folding time 12.37 days
W1
W2
W3
-0.55
-0.6
-0.65
-0.7
-0.75
-0.8
-0.85
-0.9
-0.95
-1
-1.05
-1.1

Fig. 10